Nanoscale Advances

ROYAL SOCIETY OF CHEMISTRY

PAPER

View Article Online
View Journal | View Issue

Cite this: *Nanoscale Adv.*, 2026, **8**, 1934

A novel molecularly engineered deep eutectic surfactant from a Gemini ionic liquid and methylurea for EOR utilization: a joint experimental and computational study

Shima Yaghoubi,[a] Javad Saien, *[a] Mona Kharazi, [a] Ehsan Alavipour[b] and Mehdi Bayat[c]

It is well established that surfactant-assisted enhanced oil recovery (EOR) offers significant advantages for improving oil production efficiency. In this study, a surface-active deep eutectic surfactant (DESU) was synthesized from a Gemini surface active ionic liquid (GSAIL) and methylurea in a molar ratio of 3 : 2, and its potential applications in EOR were systematically investigated. SEM and DLS analyses confirmed the nanoscale size of the synthesized material. FT-IR spectroscopy verified the successful formation of the DESU structure and its stability in the aqueous phase. Density functional theory (DFT) calculations revealed strong hydrogen-bonding interactions and electrostatic stabilization between the imidazolium unit and methylurea molecules, accounting for the pronounced surface activity and observed physicochemical behavior of the DESU. The synthesized DESU effectively reduced the oil–water interfacial tension (IFT) from 27.53 to a very-low value of 0.10 mN m^{-1} at 328.2 K, demonstrating superior performance compared with its individual precursors or their simple mixture. The experimental IFT data were successfully reproduced using the Frumkin adsorption model with reasonable parameter fitting. Moreover, the DESU promoted the formation of stable water-in-oil emulsions, achieving a maximum emulsion index of 65%, and altered the surface wettability of a quartz plate from oil-wet to water-wet, as evidenced by a contact angle change from 137° to 41°. Overall, these results demonstrate that the designed DESU exhibits remarkable interfacial properties and provides multiple advantages for enhancing the efficiency of EOR processes.

Received 19th December 2025
Accepted 25th January 2026

DOI: 10.1039/d5na01151e

rsc.li/nanoscale-advances

1. Introduction

Reduction in oil–water interfacial tension (IFT), *in situ* emulsification and wettability alteration of rocks are major contributing factors in enhanced oil recovery (EOR). In this regard, the impacts of influencing parameters have been the subject of many investigations for several decades.[1,2] A relevant well-known parameter is the capillary number, $C_a = \mu V/\gamma$, in which μ represents the viscosity of the displacing solution, V is the movement velocity and γ represents the IFT between the displacing solution and crude oil phases.[3] Oil recovery efficiency necessitates high capillary numbers[4] and its critical value falls within the range of 10^{-4}–10^{-3};[5] however, core tests have shown that at least a tenfold increase in capillary number is necessary to achieve about 80% recovery.[6] To establish higher capillary numbers, it is not feasible to increase the velocity of the displacing liquid solution due to limitations on the injection pressure. Also, the aqueous phase viscosity cannot be substantially increased because it would also result in a higher pressure drop, as dictated by Darcy's law.[7] Thus, efforts have been focused on IFT reduction, often achieved by utilizing surface-active agents.[8]

Surfactants adsorb at interfaces as their hydrophilic and hydrophobic parts direct into the matching phase, ultimately reducing the IFT and altering rock wettability. However, a major challenge for traditional surfactants is their poor stability under harsh reservoir conditions of salinity, temperature and pressure. In addition, nanosized surface-active particles exhibit superior performance in adsorbing at oil–water interfaces, forming micelles, and stabilizing emulsions compared to conventional surfactants. These materials can penetrate into rock cavities and partially block reservoir pores, thereby inhibiting the backflow of crude oil. Furthermore, surfactants facilitate the detachment of oil droplets from reservoir rock surfaces, and through cationic interactions and charge transfer, they cause dissolution of asphaltenes, enhance oil

[a]*Department of Applied Chemistry, Faculty of Chemistry and Petroleum Sciences, Bu-Ali Sina University, Hamedan, Iran. E-mail: saien@basu.ac.ir; jsaien@yahoo.com; m.kharazi@basu.ac.ir; kharazi.mona@yahoo.com*

[b]*Department of Inorganic Chemistry, Faculty of Chemistry and Petroleum Sciences, Bu-Ali Sina University, Hamedan, Iran*

[c]*School of Chemistry, College of Science, University of Tehran, Tehran, Iran*

displacement efficiency, and promote sweeping motion within the porous medium.[9]

In this regard, the use of a specific branch of ionic liquids, surface-active ionic liquids (SAILs) has attracted much attention. These compounds exhibit amphiphilic properties similar to surfactants thanks to their distinct hydrophilic head and hydrophobic tail. This allows them to self-organize at the critical micelle concentration (CMC) and display impressive surface activity. Their remarkable properties include thermal and chemical stability, low vapor pressure, and a wide liquid phase range.[10] Another advantage is their structual tunnability *via* hydrophilic and hydrophobic parts.[11] Among various surfactants, imidazolium-based Gemini surface-active ionic liquids (GSAILs) have demonstrated high efficiency in reducing IFT, promoting the formation of stable emulsions, and altering rock wettability.[12] In some cases, these GSAILs also exhibit nanoscale characteristics.[13]

Despite superior performance, SAILs are limited by cost for large-scale applications. A promising solution to this issue lies in forming deep eutectic surfactants (DESUs) by combining SAILs with urea derivatives.[1,14,15] Generally deep eutectic products consist of hydrogen bond donor (HBD) and hydrogen bond acceptor (HBA) constituents. These compounds can benefit the economic feasibility as well as ionic surface activity, leading to enhanced interfacial properties and structural stability. In recent years, DESUs based on choline chloride and urea have revealed desired potentials in reducing IFT, altering rock wettability and enhancing crude oil mobility.[1,14,15] In this regard, Kumar *et al.*[16] reported the impacts of a DESU obtained from choline chloride : urea (molar ratio of 1 : 2) on EOR. The IFT was reduced from 53.5 with pure water to 39.7 mN m^{-1} by using 0.77 mol dm^{-3} of the DESU. The IFT reduction was attributed to the enhanced hydrogen bonding and electrostatic interaction between adsorbed species at the interface. In a study by Rao *et al.*,[17] the addition of the DESU (chloride : urea molar ratio of 1 : 2) together with the CTAB co-surfactant resulted in reducing IFT from 37.81 to 21.27 mN m^{-1}. The corresponding synergistic interaction between the DESU and CTAB was attributed to enhanced hydrogen bonding and electrostatic effects at the oil–water interface, leading to improved wettability alteration towards water-wet state. Noteworthily, these systems often require co-surfactants to achieve optimal performance and exhibit limited stability under reservoir conditions.

In previous studies, the use of choline chloride–urea based DESUs[18,19] has provided ultimate IFT values which are not adequately low for an efficient EOR. Therefore, the development of high performance DESUs seems promising to attain desired interfacial properties. Here, we report the development of a novel DESU, by combining an imidazolium GSAIL, [3,3′-(hexane-1,6-dial) bis(1-butyl-1*H*-imidazol-3-ium) bromide], abbreviated as $[C_4im\text{-}C_6\text{-}C_4im][Br]_2$, and methylurea ($CH_3NHCONH_2$). The imidazolium cation, particularly the acidic hydrogen at the ring, serves as a strong HBD, while the accompanying anion (Br^-) enhances electrostatic stabilization. On the other hand, methylurea has a carbonyl group that can act as a HBA and the methyl branch improves the hydrophilic part of the DESU. These together bring about a strong amphiphilic and structurally stable product. The environmental promise of the DESU arises from its precursors, as both of them have been reported to exhibit high biodegradability and low toxicity.[20,21] Accordingly, a complementary density functional theory (DFT) analysis has been conducted to provide direct molecular-level insights into hydrogen bond formation and to evaluate the electrostatic stabilization of the DESU structure. IFT data could also be analyzed on a theoretical basis. Such an integrated framework highlights the potential of DESU systems as tunable and eco-friendly surfactants for efficient crude oil recovery.

2. Experimental

2.1. Materials and methods

The crude oil sample was from an oil field which is located in southern Iran for which, the detailed composition and properties of the oil are listed in Table 1. Additional chemicals were procured from Merck and Exir companies, all of which were of analytical grade and utilized with no further purification. Table 2 details the respective suppliers and the mass fraction purity of the chemicals used in the synthesis of the GSAIL and the DESU. Solutions of the DESU were prepared using fresh deionized water with an electrical conductivity of about 0.08 μS cm^{-1}.

FT-IR spectra were recorded by utilizing KBr pellets on a PerkinElmer spectrometer. Thin-layer chromatography (TLC) was employed to monitor the advancement of the GSAIL synthesis. To obtain NMR spectra, a Bruker Ultrashield instrument, operating at a frequency of 250 MHz, was used. The melting point of samples during DESU preparation was determined using capillary tubes and a Stuart melting point apparatus.

The IFT of crude oil and aqueous solutions containing DESU were determined by means of a Fars EOR Technol pendant drop tensiometer (CA-ES10 model) The specifics of the experimental setup are described in a prior study.[13] The IFT, in this method, is determined by analyzing the equilibrium between gravitational forces and the interfacial forces that hold each droplet in place. This evaluation is conducted *via* $\gamma = \Delta\rho g D^2/H$ equation[22] where, $\Delta\rho$ stands for the density difference between the two phases, g represents the acceleration due to gravity, D denotes the equatorial diameter of the droplet, and H refers to the shape parameter which depends on the shape factor S, as $S = d/D$, where d is the diameter of the drop measured at a distance D from the apex of the droplet. Details of the H values *versus* S are given in ref. 23.

To assess the capability for stable emulsion formation, equal volumes of crude oil and aqueous DESU solutions (2 cm^3) at a CMC of 0.48 mol dm^{-3} (as an intermediate IFT) were placed into vials. These mixtures were subjected to sonication in a SONICA 2400ETH S3 ultrasound bath operating at 40 kHz and 305 W for 30 minutes. Following sonication, the samples were allowed to rest at a constant temperature of 298.2 K for periods of one day and one week. Subsequently, the emulsion stability was quantified by calculating the emulsion index as $V_e/V_t \times 100$, where V_e denotes the volume of the emulsion phase and V_t is the total sample volume.[24] Additionally, microscopic examination

Table 1 Physicochemical properties of the used crude oil

Chemical properties		Physical properties	
Specification	Value–unit	Property	Value/unit
Saturated	54.0 wt%	°API	20.7 (—)
Aromatic	22.3 wt%	Density, at 20 °C	0.915 g cm^{-3}
Resin	6.7 wt%	Kinematic viscosity, at 70 °F	60 cSt
Asphaltene content	7.7 wt%	Viscosity, at 70 °F	55 cP
Loss at 200 °C	9.3 wt%	Viscosity, at 100 °F	44 cP
Total acid number	0.09 mg KOH per g		
Sulphur content	1.63 wt%		
Total salt	4 lbs per 1000 bbls		
Water content	Nil wt%		
Pour point	10 °F		
Flash point	70 °F		
Reid vapor pressure	12.1 psi		

Table 2 The supplier and purity percentage of the utilized chemicals

Chemical	Supplier	Purity percentage
1-Butylimidazole	Merck	>98
1,6-Dibromohexane	Merck	>97
Acetonitrile	Merck	≥99.9
Methylurea	Merck	>99
Tetrahydrofuran	Exir	>99.5

of the emulsions was conducted to evaluate dispersion of droplets. Images of these states were captured using a Nikon eclipse E200 microscope at 45× magnification on glass slides.

The IFT measuring apparatus was equipped with the functionality of contact angle measurement. Consequently, image analysis of oil drops on a solid substrate (specifically, a quartz plate) was performed and the contact angle at the interface of the three involved phases of water, oil, and quartz was recorded.

3. Results and discussion

3.1. Synthesis of the GSAIL and the DESU

The imidazolium GSAIL, [3,3′-(hexane-1,6-dial) bis(1-butyl-1*H*-imidazol-3-ium) bromide], abbreviated as $[C_4im\text{-}C_6\text{-}C_4im][Br]_2$, was synthesized in a comprehensive manner according to a protocol documented in previous studies.[25,26] The purity and structure of the GSAIL were verified through various analytical techniques including ^{1}H NMR, ^{13}C NMR, FT-IR, and melting point analysis utilizing authentic samples for comparison. The ^{1}H NMR and ^{13}C NMR spectra (Fig. S1 and S2 in the SI) exhibited only the peaks corresponding to the GSAIL product, with no signals indicative of the starting materials or by-products. Details are as follows:

^{1}H NMR (300 MHz, DMSO, δ, ppm) 0.87 (t, 6H, J = 9 Hz, CH_3), 1.74–1.83 (m, 8H, CH_2), 1.17–1.27 (m, 8H, CH_2), 4.24 (t, 8H, J = 6 Hz, CH_2), 9.61 (brs, 2H, imidazolium ring), 7.95–7.98 (m, 4H, imidazolium ring). ^{13}C NMR (75 MHz, DMSO, δ, ppm) 13.8, 25.2, 19.2, 31.8, 29.5, 49.0 (2C), 122.9 (2C), 136.5.

Dynamic light scattering (DLS) analysis was also performed for determining the hydrodynamic particle size and micelle formation in aqueous solutions. The measured values, related to the transfer of particles in the fluid, were within 0.7–4.9 nm for GSAIL particles. The graphs for typical concentrations below the CMC, are presented in Fig. S4. So, the synthetized GSAIL in both the solid state and aqueous solutions has nanometer size.

The scanning electron microscopy (SEM) image of the GSAIL (Fig. S3) reveals nearly spherical particles with a uniform distribution and an apparent nanoscale size in the range of 11.93–27.49 nm. Dynamic light scattering (DLS) analysis was also conducted to determine the hydrodynamic particle size of the GSAIL in aqueous solution. The measured hydrodynamic diameters, reflecting the diffusion behavior of particles in the fluid phase, ranged from 0.7 to 4.9 nm. The corresponding DLS profile is presented in Fig. S4. These findings confirm that the synthesized GSAIL possesses nanoscale dimensions both in the solid state and in aqueous solution.

To find the DESU composition, different samples were synthesized according to the method proposed by Abbott *et al.*[27,28] Various molar ratios of GSAIL : methylurea were gradually heated in a jacketed glass vessel to the melting point of the components while stirring magnetically. This process was continued until a transparent solution appeared. The temperature was then lowered until turbidity appeared, indicating a change in the solution's phase. The melting points of the precursors were determined to be 156.3 °C for GSAIL and 97.2 °C for methylurea. All samples were vacuum-dried prior to analysis to minimize the influence of moisture or impurities. The observed eutectic point were consistent across three independent measurements. The solid–liquid phase diagram presented in Fig. 1 depicts the formation of the DESU at a GSAIL : methylurea molar ratio of 3 : 2 yielding a DESU with a molar mass of 325.04 g mol^{-1}. GSAIL and methylurea form a number of hydrogen bonds, reducing the lattice energy and thereby resulting in very much low melting points within the eutectic range. The melting point of the DESU was 8.3 °C, indicating a stable liquid state suitable for use at conventional temperatures. The disparity in the freezing point at the eutectic composition, compared to that of an ideal mixture, as $\Delta T_f = 124.4$ °C represents the strength of the interactions between the HBD and the HBA. The higher value of ΔT_f indicates the stronger interaction between the HBD and the HBA components.

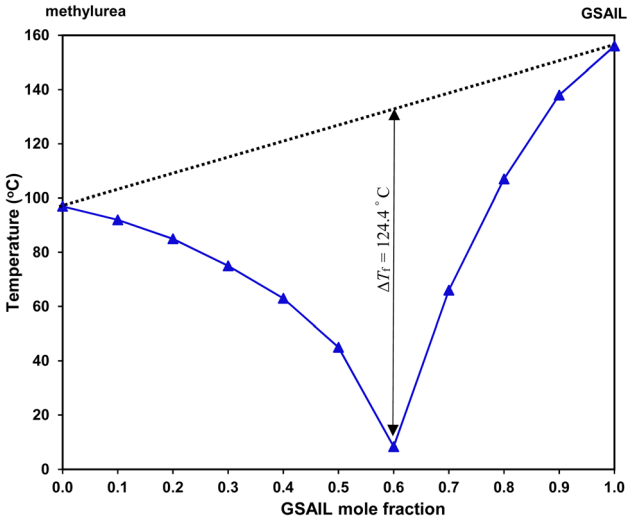

Fig. 1 Phase diagram of the DESU product from the GSAIL and methylurea precursors.

The FTIR spectra of the individual components and the synthesized DESU, as well as its aqueous solution, with 0.48 mol per dm^3 concentration, are presented in Fig. 2. In the DESU spectrum, the broad absorption band within 3200–3400 cm^{-1}, corresponding to N–H stretching vibrations (originating from methylurea), is red-shifted and significantly broadened compared to the spectrum of pure methylurea.[29] This indicates the participation of N–H groups in hydrogen bonding with electronegative acceptor sites in the GSAIL. Additionally, the C=O stretching vibration of methylurea, normally appearing near 1650 cm^{-1}, also shifts to lower wavenumbers, further supporting hydrogen bond formation.

The characteristic C–H stretching vibrations of the imidazolium ring in GSAIL (around 3100–3150 cm^{-1}) exhibit noticeable intensity variations and slight frequency shifts in the DESU spectrum. These changes suggest that the acidic hydrogen atoms of the imidazolium ring participate in hydrogen bonding interactions with the electron-rich sites of methylurea (*e.g.*, carbonyl or amine groups).[30] Furthermore, alterations observed in the fingerprint region (1000–1600 cm^{-1}) of the DESU spectrum, compared with those of the pure components, indicate the formation of a new supramolecular network stabilized through hydrogen bonding.

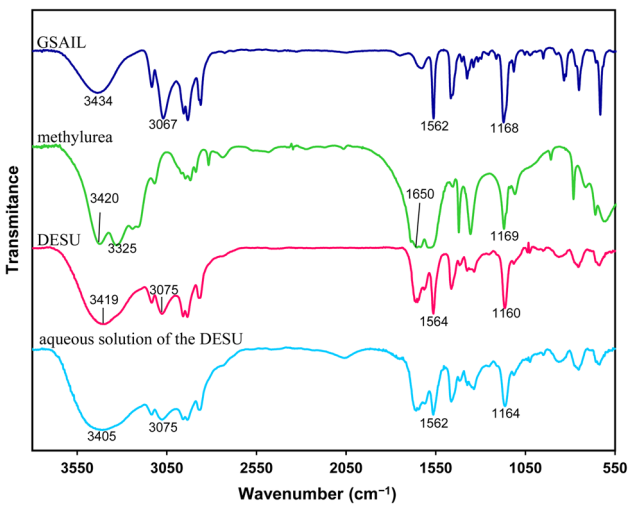

Fig. 2 FT-IR of GSAIL, methylurea, DESU and the aqueous solution of the DESU at a concentration of 0.48 mol dm^{-3}.

As is apparent for the DESU solution in water, the corresponding spectrum retains the major hydrogen-bonding of the DESU. Although minor shifts and broadening due to water interactions are expected, the characteristic bands in the 1600–1700 cm^{-1} and 3100–3400 cm^{-1} regions remain consistent, indicating that the DESU structure is preserved. Meanwhile, the absence of component-resolved peaks from GSAIL or methylurea in the aqueous spectrum suggests that no significant dissociation occurs. This structural stability enhances the practical applicability of the DESU in aqueous systems where robustness in water is important.

In Fig. 3(a), the ^1H NMR spectrum of DESU shows a singlet peak at 9.5 ppm and multiple peaks at about 7.9 ppm, attributed to the imidazolium ring protons. The broad peak at about 5.4 ppm is related to amidic protons, confirming the successful construction of the DESU *via* hydrogen bonding interactions. Moreover, the sharp peak at 2.5 ppm corresponds to the methyl group of methylurea. The triplet peak at 4.19 ppm is also attributed to the hexyl chain adjacent to the imidazolium ring. Other hydrogens of the butyl and hexyl chains with correct integrations can be observed in the range of 0.82–1.84 ppm. In Fig. 3(b) ^{13}C NMR spectrum of the DESU shows a distinctive peak at 159.98 ppm corresponding to the C=O group of methylurea. The other peaks at 136.45 and 122.87 ppm are related to the imidazolium ring. In addition, the signals of methyl, butyl and hexyl chains appear at 48.98, 31.74, 29.47, 26.65, 25.15, 19.2, and 13.71 ppm.

3.2. Computational study

The integration of theoretical calculations for experimental results is essential to reveal the molecular origin of the observed interfacial behavior. Theoretical analyses provide fundamental insights into hydrogen bonding, charge transfer, and electrostatic stabilization within the DESU structure, thereby offering a clear mechanistic explanation for its superior surfactant performance.

The DESU structure, comprising six imidazolium cations, six bromide anions and two methylurea molecules, was investigated at the CAM-B3LYP-D3 level of theory. For simplicity, the system here is denoted as $([LH_2]^{2+}[Br_2]^{2-})_3[MU]_2$, where $[LH_2]^{2+}[Br_2]^{2-}$ represents the GSAIL and [MU] represents the methylurea units. Geometry optimization was performed in the gas phase using the CAM-B3LYP-D3 functional with the def2-SVP basis set. Subsequently, natural bond orbital (NBO), energy decomposition analysis (EDA) and atoms in molecules (AIM) calculations were carried out at the CAM-B3LYP/Def2-TZVP level of theory. The resulting optimized geometries are presented in Fig. 4 where the key bond lengths and bond angles involved in the interactions are presented.

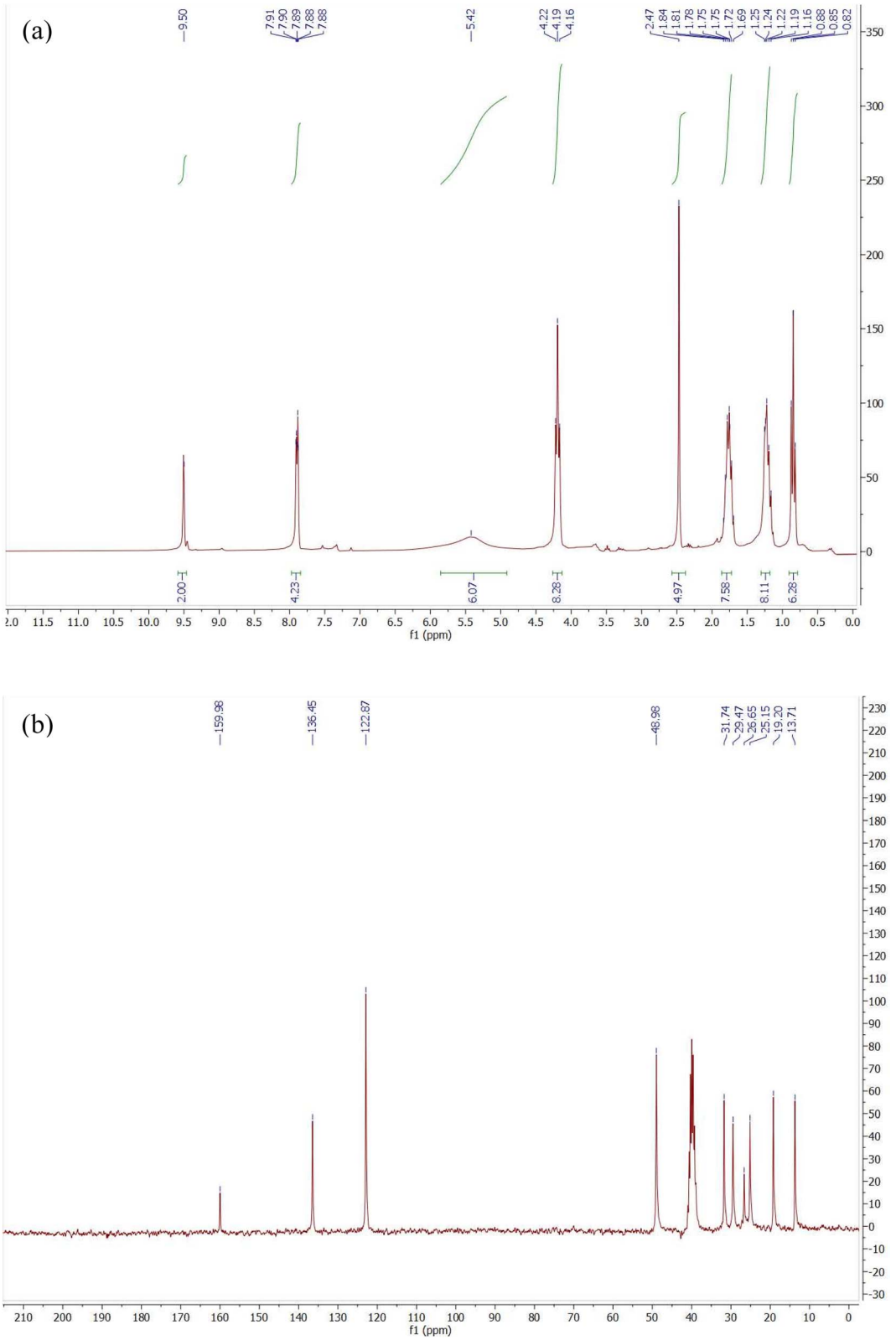

Fig. 3 The ^{1}H NMR spectra (a) and ^{13}C NMR spectra of the DESU (b).

The NBO method converts delocalized molecular orbitals into localized ones, providing a clear picture of bonds, lone pairs, bond orders, charges, and donor–acceptor interactions. It bridges quantum mechanical results with classical chemical concepts, making it especially useful for studying bonding, molecular stability, hyperconjugation, hydrogen bonding, and

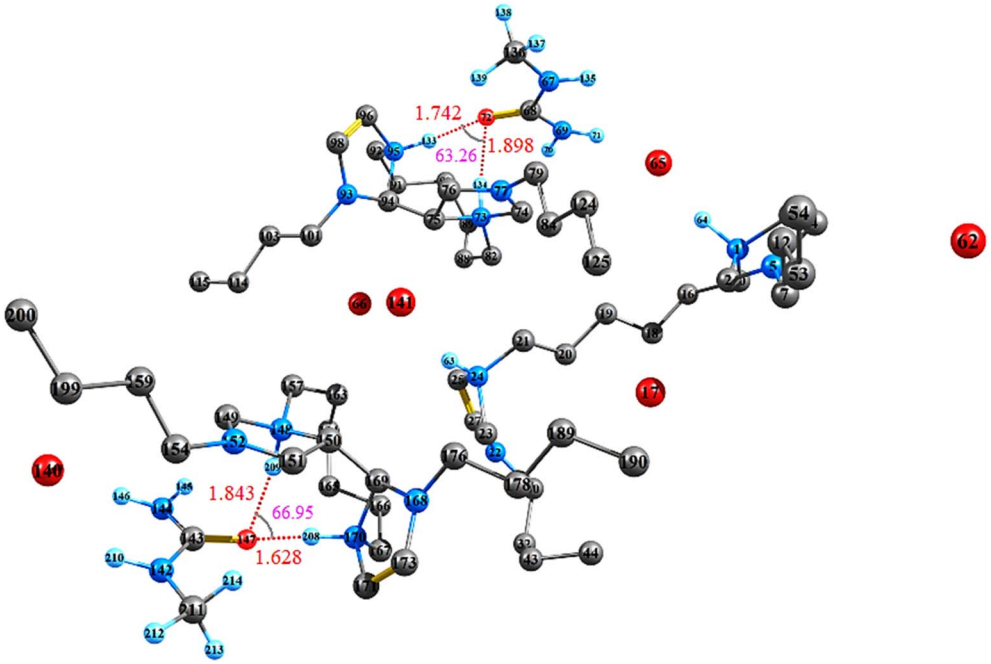

Fig. 4 Optimized geometry of the DESU structure at the B3LYP-D3/def2-SVP level, showing atom numbering along with the key bond lengths (Å) and bond angles involved in interaction. For clarity, all hydrogen atoms, except for the positively charged hydrogens and those attached to the methylurea group, have been omitted.

reaction mechanisms.[31,32] The analysis includes the Wiberg bond index (WBI),[33,34] natural atomic charge transfer,[35] and the key donor–acceptor interactions.[36] NBO analysis was carried out at the CAM-B3LYP-D3/Def2-SVP//CAM-B3LYP-D3/Def2-TZVP level of theory for the DESU structure.

The WBI, derived from NBO analysis, serves as a numerical descriptor of bond order. In this study, the O···H bond orders of the studied structures were calculated at the CAM-B3LYP-D3/Def2-SVP//CAM-B3LYP-D3/Def2-TZVP level of theory. The resulting bond orders and corresponding bond lengths are presented in Table 3. The optimized structure reveals an intramolecular O···H bond interaction between methylurea and the N–H fragment of imidazolium in the optimized structure. These findings are consistent with the Wiberg index values calculated for the interacting fragments in the DESU structure.

The partial charges on the oxygen and hydrogen atoms involved in the O···H interaction, as well as the charge redistribution between the two investigated fragments, are summarized in Table 4. The results confirm a charge transfer of approximately $-1.6e$ from GSAIL to the two methylurea molecules within the DESU structure. The natural charges calculated for the two oxygen atoms and four hydrogen atoms are presented as averaged values, each corresponding to a single oxygen and a single hydrogen atom, respectively.

Generally, donor–acceptor interactions are stabilized due to electron density delocalization from a filled donor orbital into an empty acceptor orbital. NBO analysis quantifies this effect using second-order perturbation theory, providing insight into hyperconjugation, back-donation, and charge transfer in molecular systems.[37] The most significant donor–acceptor interaction between fragments in the DESU structure, arises from the charge transfer from the lone pairs of oxygen atoms of methylurea to adjacent antibonding orbitals (σ*) of the N–H fragment of imidazolium. Oxygen atoms primarily interact with N–H bonds, with the strongest stabilization (21.38 kcal mol) resulting from $O_{147} \rightarrow N_{70}–H_{208}$ transfer. These interactions reinforce weak bonds like hydrogen bonds, thereby enhancing the overall molecular stability as reflected in Table 5.

The interaction energy between the two investigated units, *i.e.* $([LH_2]^{2+}[Br_2]^{2-})_3$ as unit A and $[MU]_2$ as unit B in the DESU structure was evaluated based on the following equation[38] at the CAM-B3LYP-D3/Def2-SVP//CAM-B3LYP-D3/Def2-TZVP level of theory.

$$IE_{AB} = E_{AB} - (E_A + E_B) \quad (1)$$

Table 3 The Wiberg index and calculated O···H bond lengths according to Fig. 4

$O_{72}–H_{134}$	$O_{72}–H_{135}$	$O_{147}–H_{208}$	$O_{147}–H_{209}$
Wiberg index			
0.057	0.044	0.09	0.053
Bond length (Å)			
1.74	1.90	1.63	1.84

Table 4 Natural charge and the amount of charge transfer for the DESU structure

Natural charge		Charge transfer
O	H^+	$([LH_2]^{2+}[Br_2]^{2-})_3 \rightarrow [MU]_2$
$-0.8e$	$0.46e$	$-1.6e$

Table 5 Most important donor–acceptor interactions analysis in the DESU structure

Donor → acceptor	Type	E (kcal mol^{-1})
$O_{72} \rightarrow N_{73}$–$H_{134}$	LP → σ*	3.61
$O_{72} \rightarrow N_{95}$–$H_{133}$	LP → σ*	19.71
$O_{147} \rightarrow N_{70}$–$H_{208}$	LP → σ*	21.38
$O_{147} \rightarrow N_{148}$–$H_{209}$	LP → σ*	10.04

The results, in good agreement with NBO data, show the existence of an interaction energy of about −99.61 kCal mol^{-1} between the investigated fragments in the DESU structure.

Energy decomposition analysis (EDA) is a powerful computational tool used to investigate the nature of chemical bonding in molecules and complexes. EDA breaks down the total interaction energy between two units into physically meaningful components, electrostatic interaction ΔE_{elstat} and classical coulombic attraction between unit charge distributions. Pauli repulsion ΔE_{Pauli} destabilizes interactions due to electron cloud overlap and the Pauli exclusion principle. Orbital covalent interaction, ΔE_{orb}, in turn, stabilizes effects arising from electron sharing, charge transfer, and polarization. Dispersion interaction, ΔE_{disp}, represents the dispersion energy contribution, accounting for weak van der Waals interactions arising from correlated electron motion between fragments.[39] Accordingly, the interaction energies between the N–H fragment of imidazolium units and methylurea in the DESU structure were computed using ADF 2013 at the BP86-D3/TZP level of theory. These energies were decomposed according to the following equation:[39]

$$\Delta E_{\text{int}} = \Delta E_{\text{elstat}} + \Delta E_{\text{pauli}} + \Delta E_{\text{orb}} + \Delta E_{\text{disp}} \quad (2)$$

The corresponding results are summarized in Table 6, indicating excellent agreement with the interaction energies obtained from the Gaussian calculations. The EDA results confirm that, electrostatic contributions are dominant, suggesting that the O···H bond interactions between the interacting fragments in the DESU structure play a key role.

Bond critical points (BCPs) between interacting fragments in the DESU structure were analyzed using Bader's AIM theory.[40] Topological parameters at these points, including the electron density (ρ) and the Laplacian of the electron density, $\nabla_\rho^2(r_c)$, were calculated for the O···H bonds in the DESU structure. The results are summarized in Table 7. A low electron density (ρ < 0.1 au) combined with a positive Laplacian, $\nabla_\rho^2(r_c)$, confirms van der Waals interactions in the O···H bonds.

The above DFT calculations elucidated the enhanced amphiphilicity of the designed DESU. Charge transfer analysis indicated a pronounced electron donation from methylurea to the imidazolium unit, which increases the polarity and hydration capacity of the headgroup. Furthermore, the results highlighted the dominant contribution of electrostatic and orbital interactions in stabilizing the hydrophilic domain, while the hydrophobic alkyl chains of the GSAIL remained free to interact with the oil phase. AIM analysis confirmed the presence of stable hydrogen bonds between the imidazolium headgroups and methylurea, with significant bond order and short bond lengths, reinforcing the hydrophilic character of the polar region. These collectively confirm the superior amphiphilic nature of the DESU.

Table 7 Topological properties (a.u.) for the DESU structure

Bond	$\rho(r_c)$	$\nabla_\rho^2(r_c)$
O_{72}–H_{133}	0.052	0.13
O_{72}–H_{134}	0.056	0.11
O_{147}–H_{208}	0.068	0.12
O_{147}–H_{209}	0.058	0.11

3.3. IFT variation

The IFT variations of the considered system in the presence of the DESU (GSAIL : methylurea molar ratio of 3 : 2), were investigated. The IFT measurements were performed at ambient pressure and various temperatures. Fig. 5 illustrates the relationship between IFT and the concentration of the DESU. It is evident that IFT decreases with DESU concentration, even at low concentrations and continues until reaching the CMC. This phenomenon can be attributed to the amphiphilic characteristics of the GSAIL-based DESU, which has a tendency to adsorb at the interface between organic and aqueous phases.[41] Upon reaching the interface, the hydrophobic lateral chains and spacer chains of the DESU molecules preferentially position themselves within the oil phase. Meanwhile, the hydrophilic imidazolium rings exhibit strong electrostatic interactions with water and tending to remain in the aqueous phase (Fig. 6).[42] Methylurea increases the polarity and hydration of the GSAIL head group region, improving its ability to align with water molecules and displace water from the interface, a key step in reducing IFT.[43]

In a study, by Rao *et al.*,[17] it has been shown that upon addition of a commercial co-surfactant (cetyltrimethyl ammonium bromide, CTAB) to a 0.07 mol per dm^3 solution of choline chloride : urea (1 : 2) DESU, the amount of IFT reduction was only 16.54 mN m^{-1} at a temperature of 303 K. The synergistic interaction between DESU and CTAB was attributed to enhanced hydrogen bonding and electrostatic effects at the oil–water interface, leading to improved wettability transition toward a water-wet state. This is while the employed imidazolium-based DESU in this study, could give a low IFT of 0.83 mN m^{-1} at 298.2 K, at a concentration of 0.48 mol dm^{-3} and without using a co-surfactant.

Table 6 EDA (kcal mol^{-1}) of the DESU structure at the BP86-D3/TZP level

Fragment	ΔE_{Pauli}	ΔE_{elstat}	ΔE_{orb}	ΔE_{disp}	ΔE_{int}
A–B	138.03	−119.77 (49.7%)	−85.60 (35.5%)	−35.72 (14.8%)	−103.07

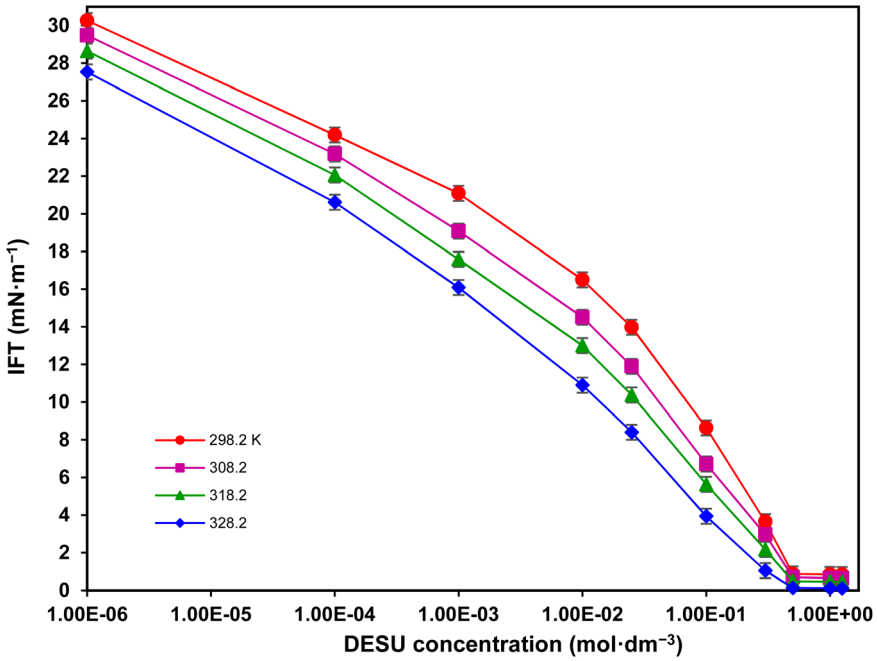

Fig. 5 IFT variations as a function of the DESU concentration at different temperatures.

Additionally, as presented by Fig. 5, temperature favors IFT reduction which can be attributed to the following reasons:[44]

• Interrupting the surrounding water molecules around the hydrophilic regions of the DESU which diminishes the aqueous phase solubility and favors its adsorption.

• Favoring molecular motion and reducing the intermolecular forces at the interface.

• Decreasing the aqueous phase viscosity which facilitates mass transfer from the bulk solution, thereby promoting adsorption of the DESU.

Table 8 presents the relevant values of clean system IFT (no surfactant addition), CMC, IFT at the CMC, and the maximum IFT reduction for the utilized DESU at various temperatures. The DESU shows the lowest IFT value of 0.10 mN m^{-1} at a CMC of 0.41 mol dm^{-3} at 328.2 K. The relatively high CMC can be attributed to the bulky Gemini headgroup and strong hydrogen-bonding interactions in the DESU system, which reduce aggregation tendency at low concentrations. Noteworthily each CMC was determined from the intercept of tangential lines before and after the zone where the IFT data tend to a constant value.[40]

To comprehensively evaluate the performance of the DESU, IFT variations were measured for the individual precursors (GSAIL and methylurea) and for their simple mixture at a 3 : 2 molar ratio (no DESU formation), all at 298.2 K. As illustrated in Fig. 7, at CMC concentrations of about 0.5 and 1.0 mol dm^{-3} with individual components of methylurea and GSAIL, minimum IFT values of 14.72 and 11.49 mN m^{-1} were achieved. In contrast, their mixture was able to reduce the IFT to 7.57 mN m^{-1}. However, in comparison, the DESU with a CMC of 0.48 mol dm^{-3} brings about a minimum IFT as low as 0.83 mN m^{-1}.

In prior studies with the same crude oil and at the consistent temperature of 298.2 K, IFT values of 1.55 and 1.21 mN m^{-1} were recorded utilizing the conventional surfactants of sodium dodecyl sulfate (SDS) and sodium dodecyl benzene sulfonate (SDBS) at concentrations of 0.25 and 0.20 mol dm^{-3}, respectively.[45,46] However, in the current study, an IFT value of 5.40 mN m^{-1} corresponded to a DESU concentration of 0.20 mol dm^{-3}, suggesting that conventional surfactants exhibit better performance at moderate concentrations. This is while at a higher concentration of 0.48 mol dm^{-3} (CMC of the DESU), the performance of the DESU becomes comparable, as the IFT reaches 0.83 mN m^{-1}; whereas the corresponding values with SDS and SDBS are 1.1 and 1.2 mN m^{-1}, respectively. Thus, the IFT reduction achieved by the DESU is superior to that reported for conventional surfactants like SDS and SDBS under comparable conditions, highlighting its practical competitiveness. It is important to note that the environmental benefits, associated with the use of the DESU, should also be considered.

3.4. Theoretical DESU adsorption study

The well-known Frumkin adsorption isotherm effectively represents the experimental IFT data at concentrations lower than the CMC across the different studied temperatures. This isotherm accounts for the non-ideal interactions (either attractive or repulsive) between adsorbed species at the interfaces.[47] The corresponding equation of state and the isotherm are as follows:[48]

$$\Pi = -2RTT_{m,F}[\ln(1-\theta) + \beta\theta^2] \quad (3)$$

$$b_F f_{\pm}\left[C\left(C + C_{electrolyte}\right)\right]^{1/2} = \frac{\theta}{1-\theta}\exp(-n\beta\theta) \quad (4)$$

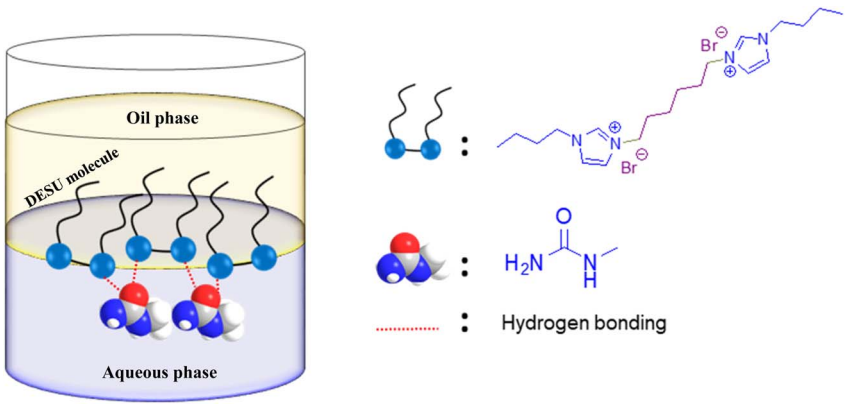

Fig. 6 The schematic of the DESU orientation in the oil–water system.

In these equations, $\Pi = \gamma_o - \gamma$, refers to interfacial pressure, γ_o is the IFT of the pure system (no surfactant present) and γ is the measured IFT under a specific condition *i.e.* when surfactant is present at a certain concentration. Additionally, $\theta = \Gamma/\Gamma_{m,F}$ represents the fraction of the interface covered by the surfactant. Other parameters are relevant to the Gibbs dividing interface theory,[48] which underpins the Frumkin isotherm. These encompass the maximum interfacial excess concentration as described by the Frumkin model, $\Gamma_{m,F}$, the activity coefficient of ions, $f_{\pm}$, the van der Waals molecular interaction parameter, β, and the Frumkin adsorption constant, b_F. To assess the accuracy of fitting the experimental data to the Frumkin isotherm, the following objective function (OF) was calculated:[49]

$$\mathrm{OF} = \sum_{i=1}^{m} \frac{\Delta C_i}{C_{exp,i}} \frac{\Delta \Pi_i}{\Pi_m - \Pi_1} \quad (5)$$

where $\Delta C_i = |C_{exp,i} - C_{cal,i}|$ and $\Delta \Pi_i = (\Pi_{i+1} - \Pi_{i-1})/2$ represent the deviations between the experimentally determined and calculated concentrations and interfacial pressure values corresponding to the ith data point. Additionally, $\Pi_m = \gamma_o - \gamma_m$ refers to the highest interfacial pressure in relation to γ_m, the final IFT in a dataset comprising m data points. The calculations were performed using IsoFit software. Fig. S5 shows that the Frumkin adsorption isotherm aligns well with the data for a typical temperature of 298.2 K. Consequently, the fitting parameters and the corresponding OF values were determined as listed in Table 9. The OF values, ranged from 0.22 to 0.46 within the temperature range, confirming that the fits were satisfactory.

The $\Gamma_{m,F}$ values of the DESU are of the same order as those previously reported for a number of surface active agents.[18] This can be explained by the increased hydrophobicity and adsorption propensity. Meanwhile, negative values of β indicate electrostatic repulsive forces among the adsorbed DESU molecules. Similarly, a more compact interfacial arrangement of adsorbed molecules, observed at elevated temperatures, indicates an increase in electrostatic repulsion, as reflected by higher β values. In contrary, the Frumkin adsorption equilibrium constant (b_F) decreases with rising temperature, consistent with the enhancement of electrostatic repulsion at elevated temperatures. Notably, the minimum occupied surface area by each adsorbed molecule, A_m, is expressed as:

$$A_m = 1/(\Gamma_{m,F} N_{AV}) \quad (6)$$

where N_{AV} represents Avogadro's number. An increase in temperature elevates the interfacial concentration, promoting a more compact arrangement of particles within the adsorption layer. Consequently, this results in a relatively smaller area occupied by each molecule, denoted as A_m. As observed, the parameter $\Gamma_{m,F}$ exhibits an increase with temperature. This phenomenon can be attributed to the enhanced mobility of the DESU molecules as well as dehydration of their hydrophilic regions within the bulk phase.

The corresponding thermodynamic parameters of ΔG°_{ads} and ΔG°_{mic}, which pertain to the adsorption and micellization Gibbs free energies, indicating the tendencies for adsorption and aggregation, are stated as:[49,50]

$$\Delta G^{\circ}_{ads} = -2RT \ln\left(\frac{b_F \rho'}{2}\right) \quad (7)$$

$$\Delta G^{\circ}_{mic} = RT \ln \mathrm{CMC} \quad (8)$$

Table 8 The relevant parameters of IFT reduction with the used DESU at various temperatures

T (K)	CMC (mol dm^{-3})	IFT of clean system, γ_0 (mN m^{-1})	IFT at CMC, γ_{CMC} (mN m^{-1})	Minimum IFT γ_{min} (mN m^{-1})	Maximum IFT reduction (%)
298.2	0.48	30.26	0.86	0.83	97.2
308.2	0.45	29.47	0.69	0.64	97.8
318.2	0.42	28.64	0.48	0.44	98.4
328.2	0.41	27.53	0.13	0.10	99.6

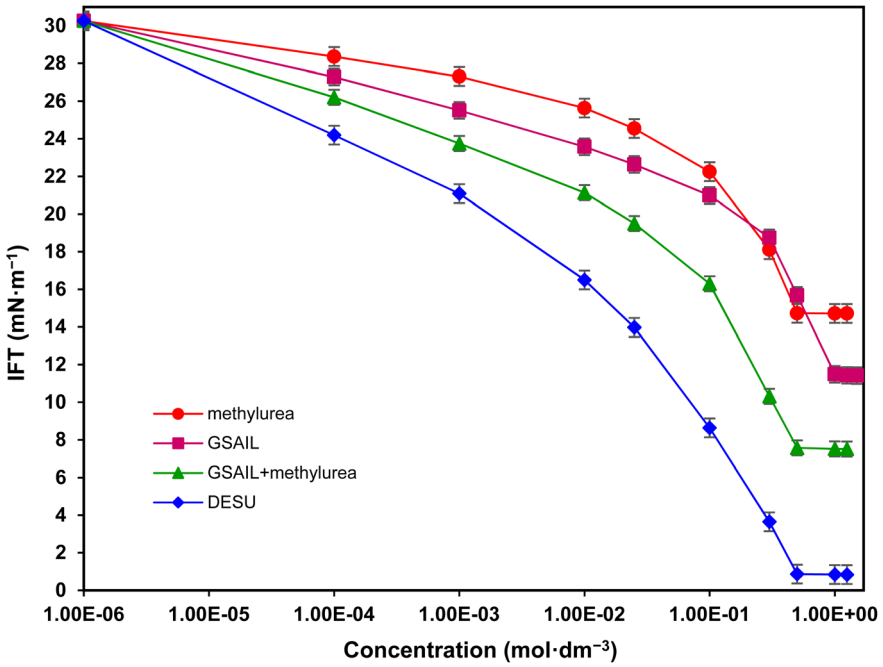

Fig. 7 Variation of the IFT between crude oil–water as a function of DESU concentration and the individual precursors at 298.2 K.

where the water molar concentration is represented by $\rho' = \rho/18$. The data presented in Table 9 demonstrate that the negative values of Gibbs free energy signify the spontaneous nature of both the adsorption and micellization of the DESU at the crude oil–water interface and in the aqueous phase, respectively. Notably, the broader distribution of molecular charge contributes to stronger interactions for the DESU. At elevated temperatures, increased thermal mobility results in a rise in the adsorption free energy. Additionally, the dehydration of the hydrophilic components of the DESU in the bulk phase enhances their tendency to aggregate with increasing temperature. Sensibly, the absolute values of ΔG°_{ads} are significantly higher than those of ΔG°_{mic}, suggesting a preference of the DESU to adsorb rather than to form aggregates in the bulk phase.

Finally, changes in interface entropy, denoted as ΔS, along with the changes in energy, ΔU, were determined using the following equations:[51]

$$\Delta S = -\left(\frac{\partial \gamma}{\partial T}\right)_{p,C} \quad (9)$$

$$\Delta U = \gamma + T\Delta S \quad (10)$$

The variations of ΔS and ΔU as functions of temperature are illustrated in Fig. S6 and S7, respectively. Variations of ΔS can be attributed to the alternative phenomena of enhanced agitation and dehydration of the DESU molecules.[52] The former phenomenon leads to higher entropy, while the latter results in significant van der Waals attraction, thereby reducing the entropy values.[53] A similar trend is observed for the energy, ΔU, in relation to ΔS.

The strong hydrogen bonding and charge transfer interactions, revealed by DFT calculations, are consistent with the non-ideal adsorption behavior characterized by dominant interactions between the adsorbed molecules and quantified by the Frumkin model. In this model, lateral interactions between adsorbed DESU molecules at the oil–water interface are taken into account.

3.5. Investigating the emulsification capability

In the context of crude oil extraction, it is essential to facilitate the transfer of surfactants to low permeable reservoir zones and to dissolve residual crude oil by creating emulsions. Emulsions enhance the movement of fluids in regions that have not been effectively swept, obstruct permeable zones to prevent the backflow of crude oil, and significantly increase the mobility.[54] Indeed, a low IFT is crucial for the development of stable emulsions.

Fig. 8 displays the images of crude oil–water emulsions containing 0.48 mol dm^{-3} of the DESU, captured after one day and one week, accompanied by the respective microscopic photographs. Accordingly, Fig. 9 shows that the emulsification

Table 9 Obtained parameters based on the Frumkin isotherm at different temperatures for DESU

T (K)	$\Gamma_{m,F} \times 10^6$ (mol m^{-2})	β	b_F (dm^3 mol^{-1})	OF	$A_m \times 10^{36}$ (m^2)	ΔG°_{ads} = (kJ mol^{-1})	ΔG°_{mic} = (kJ mol^{-1})
298.2	1.81	−9.9	46 270	0.22	6.40	−69.68	−1.81
308.2	2.04	−11.0	45 792	0.38	5.70	−71.95	−2.04
318.2	2.38	−13.3	45 174	0.47	4.88	−74.18	−2.29
328.2	2.63	−14.7	44 288	0.46	4.42	−76.37	−2.49

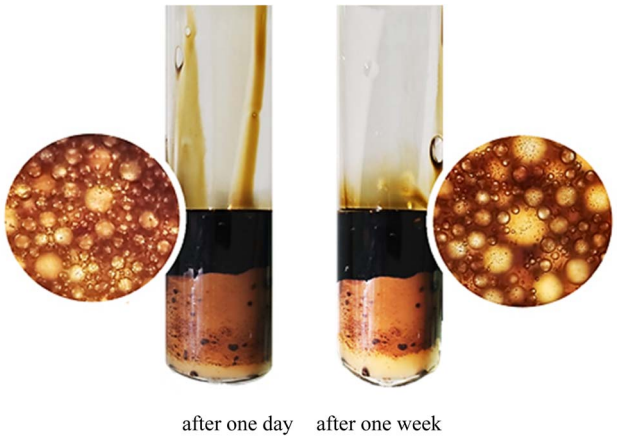

Fig. 8 The crude oil–water emulsions and the microscopic images (45× magnification) with 0.48 mol dm^{-3} of the DESU at 298.2 K.

index for the DESU reaches a maximum of 65% after one day and 52% after one week. Furthermore, the microscopic images demonstrate that the DESU facilitates a nearly uniform distribution of water droplets in crude oil. Also, stable emulsions were formed in the presence of the DESU with the size of droplets ranging from 5–90 μm after one day and 7–110 μm, after one week, respectively. This can be attributed to the pronounced amphiphilic characteristics of the DESU and the rather long hydrophobic alkyl chain of the GSAIL provides steric stabilization within the oil phase, preventing droplet coalescence. The probable formation of a coherent and elastic interfacial film could also reduce the interfacial mobility and promote kinetic stability of the emulsion.

3.6. Investigating the wettability alteration

The affinity of a rocks' surface to crude oil or water is recognized as a critical parameter when both fluids are in contact with the rock. The separation of residual oil from reservoir rocks is facilitated by a transition in wettability from oil-wet to water-wet, thereby improving EOR. Reservoirs are accordingly categorized into hydrophilic (water-wet) with contact angles within 0–80°, intermediate within 80–100°, and hydrophobic (oil-wet) within 100–180°.[55] It should be noted that, in the case of an oil drop forming within an aqueous medium, the external angle that is established at the interface with the surrounding aqueous phase is considered as the contact angle.

Fig. 10 displays the shape of attached drops in DESU solutions on a quartz surface, along with the measured contact angles at 298.2 K. The contact angle was initially measured at 137° in the absence of DESU, indicating an oil-wet surface. This significantly decreased to 41° at a concentration of 0.48 mol dm^{-3} of the DESU. The variations clearly indicate that the solution of DESU successfully modifies the surface wetting affinity to a water-wet state. The hypothesized mechanism underlying this observation suggests that in addition to crude oil drops, the DESU could aggregate on the solid surface. In this arrangement, the alkyl chains orient themselves towards the surface of the plates, while the polar components are directed towards the surrounding solution. Methylurea, acting as a hydrogen bond donor, promotes the formation of a stable hydrogen-bonding network at the solid–liquid interface. This configuration enhances the hydrophilicity of the plates, facilitating the separation of trapped oil and resulting in a transition from an oil-wet surface to a water-wet state. This transition increases with the concentration of the DESU.[56]

The observed wettability alteration can be attributed to the strong interaction of the DESU molecules with the quartz

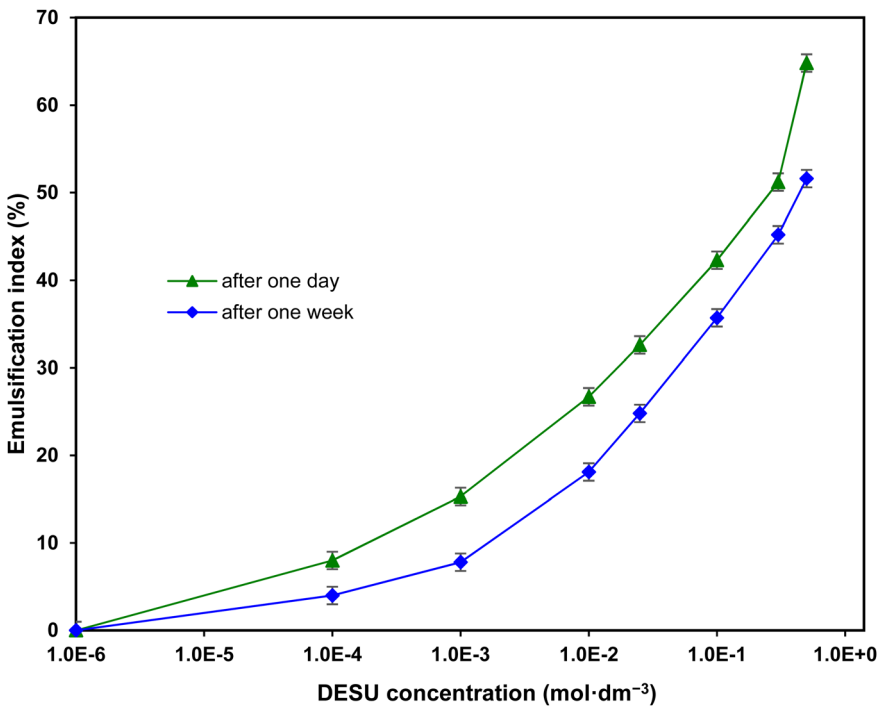

Fig. 9 The emulsion index *versus* DESU concentration at 298.2 K.

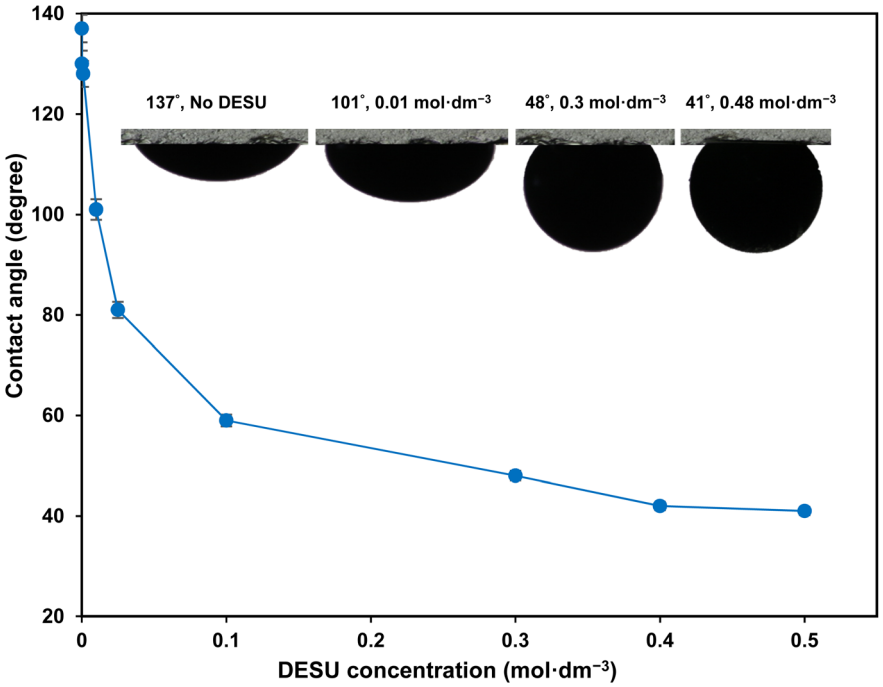

Fig. 10 Contact angle of crude oil surrounded by different DESU aqueous solutions on a quartz surface at 298.2 K.

surface. Under near-neutral pH conditions, the quartz substrate carries negatively charged Si–O$^-$ groups that interact electrostatically with the cationic headgroup, present in the DESU.[57]

The results are consistent with those reported by Guo *et al.*,[58] who investigated a DESU composed of choline chloride and urea (molar ratio 1 : 2) applied to Indiana limestone core plugs. In their study, the contact angle decreased from 137.0° to 54.3° upon using 0.5 mol dm^{-3} of the DESU. However, this reduction was less pronounced than that achieved by the DESU employed in the present work. This comparison, supported by molecular-level interaction analyses, highlights the significance of rationally designing DESU structures. In particular, the findings underscore that selecting an appropriate HBD is essential for optimizing wettability alteration processes in EOR applications.

Notably, the DFT calculations are consistent with and support the above explained experimental observations. The computed charge transfer and strong O···H hydrogen bonds enhance the polarity and stability of the DESU headgroup, giving rise the adsorption capability at the oil–water interface. The high interaction energies (Table 6) confirm the stability of the DESU, consistent with the observed micellization and emulsion formation. Moreover, AIM analysis highlights electrostatic and orbital contributions that strengthen the hydrophilic domain, rationalizing the wettability alteration of quartz from oil-wet to water-wet.

4. Conclusions

In this study, a novel deep eutectic surfactant was developed by combining an imidazolium-based Gemini surface active ionic liquid and methylurea, aiming to generate an efficient surfactant to improve the interfacial phenomena involved in the EOR process. In addition to the conventional analysis, the theoretical calculations provided deep insight into the molecular origin of the amphiphilicity of the target product. NBO analysis showed effective charge transfer and EDA emphasized electrostatic and orbital stabilization. AIM analysis confirmed strong hydrogen bonding between the imidazolium unit and methylurea, reinforcing the hydrophilic region.

Interestingly, the IFT reached the 0.10 mN m^{-1} value at 328.2 K, *i.e.* acting much stronger than individual constituents and achieved without using co-surfactants. Consequently, the Frumkin adsorption model was employed to precisely reproduce the obtained data and to facilitate the determination of the associated parameters. The emulsification study indicated that the DESU could disperse water droplets, forming stable water-in oil emulsion that remained stable over a one-week period. Furthermore, the solid surface wettability was altered from oil-wet to water-wet in the presence of the DESU as a consequence of reduced adhesion between crude oil and the solid surface. This transition was attributed to the effective adsorption of the DESU at the solid surface.

Overall, the DESU with its unique molecular structure and interfacial activity presents a promising alternative to conventional surfactant systems for EOR. Future studies could focus on scaling up the system, conducting core flooding experiments to directly confirm the oil recovery potential of the DESU, and testing its performance under reservoir-relevant salinity and hardness conditions as well its long-term stability under high-salinity brine conditions.

Author contributions

Shima Yaghoubi: experiments, methodology, visualization, software, data curation, original draft preparation. Javad Saien:

supervision, methodology, funding acquisition, formal analysis, writing – review and editing. Mona Kharazi: visualization, investigation, software, writing initial draft. Ehsan Alvaipour: software, original draft preparation. Mehdi Bayat: software, methodology.

Conflicts of interest

The authors declare that they have no known competing financial interests or personal relationships that could have appeared to influence the work reported in this paper.

Data availability

The data supporting this article have been included as part of the supplementary information (SI). Supplementary information: structural, morphological, colloidal, and thermodynamic characterization data related to the prepared deep eutectic surfactant (DESU). The ^{1}H NMR and ^{13}C NMR spectra (Fig. S1 and S2) confirm the chemical structure of 3,3'-(hexane-1,6-diyl) bis(1-butyl-1*H*-imidazol-3-ium) bromide. The SEM image (Fig. S3) illustrates the surface morphology of the synthesized compound. DLS analysis (Fig. S4) evaluates the aggregation behavior and particle size distribution at two representative concentrations, measured before and after the CMC under natural pH at 298.2 K. The experimental data fitting with the Frumkin adsorption isotherm (Fig. S5) is presented to analyze the interfacial adsorption behavior. Additionally, the temperature dependency of thermodynamic parameters, including entropy change and energy change of the DESU adsorption (Fig. S6 and S7), is presented to provide insight into the nature and driving forces of the adsorption process. See DOI: https://doi.org/10.1039/d5na01151e.

Acknowledgements

The authors would like to acknowledge Bu-Ali Sina University for the financial support of this research.

References

1 D. S. Raut, V. A. Joshi, S. Khan and D. Kundu, A priori screening of deep eutectic solvent for enhanced oil recovery application using COSMO-RS framework, *J. Mol. Liq.*, 2023, **377**, 121482.
2 S. M. Seyyedsar and M. Sohrabi, intermittent CO_2 and viscosity-reducing gas (VRG) injection for enhanced heavy oil recovery, *Fuel Process. Technol.*, 2017, **164**, 1–12.
3 G. Dordzie and M. Dejam, Enhanced oil recovery from fractured carbonate reservoirs using nanoparticles with low salinity water and surfactant: A review on experimental and simulation studies, *Adv. Colloid Interface Sci.*, 2021, **293**, 102449.
4 J. Saien and M. Kharazi, Chemical Enhanced Oil Recovery Using Ionic Liquid-Based Surfactants, in *Surfactants: Fundamental Concepts and Emerging Perspectives*, ed. O. Owoseni, IntechOpen, 2023.
5 L. Gong, G. Liao, H. Luan, Q. Chen, X. Nie, D. Liu and Y. Feng, Oil solubilization in sodium dodecylbenzenesulfonate micelles: New insights into surfactant enhanced oil recovery, *J. Colloid Interface Sci.*, 2020, **569**, 219–228.
6 M. Shakeel, A. Samanova, P. Pourafshary and M. R. Hashmet, Capillary desaturation tendency of hybrid engineered water-based chemical enhanced oil recovery methods, *J. Energy*, 2021, **14**, 4368.
7 M. S. Kamal, I. A. Hussein and A. S. Sultan, Review on surfactant flooding: Phase behavior, retention, IFT, and field applications, *Energy Fuel.*, 2017, **31**, 7701–7720.
8 L. Jangid, K. Ojha and A. Mandal, Application of green Gemini surfactants synthesized from Brassica juncea for enhanced oil recovery from high saline and high temperature reservoirs, *J. Taiwan Inst. Chem. Eng.*, 2026, **179**, 106462.
9 R. A. El-Nagar, M. I. Nessim, D. A. Ismail, M. G. Mohamed and A. Ghanem, Investigation the effect of different ionic liquids based-aryl imidazole on the onset precipitation of asphaltene, *Sci. Rep.*, 2023, **13**, 4054.
10 P. Pillai and A. Mandal, Synthesis and characterization of surface-active ionic liquids for their potential application in enhanced oil recovery, *J. Mol. Liq.*, 2022, **345**, 117900.
11 M. Kharazi, J. S. A. Javadi and R. Miller, *Innovations in Ionic Liquid-Based Surfactants and Interfacial Phenomena*, CRC Press, Boca Raton, 2025, ISBN: 9781032748078.
12 J. Saien, A. Eghtenaei and M. Kharazi, Qualifying interfacial properties of crude oil–water system with the synergistic action of a nano Gemini ionic liquid and conventional surfactants, *J. Sci. Rep.*, 2024, **14**, 19833.
13 S. Asadabadi, J. Saien and M. Kharazi, Enhanced interfacial activity by maximizing synergy between long-chain ionic liquid and conventional surfactant for enhanced oil recovery, *RSC Adv.*, 2024, **14**, 18942–18949.
14 A. Mohsenzadeh, Y. Al-Wahaibi, R. Al-Hajri, B. Jibril and N. Mosavat, Sequential deep eutectic solvent and steam injection for enhanced heavy oil recovery and in-situ upgrading, *Fuel*, 2017, **187**, 417–428.
15 M. Atilhan and S. Aparicio, Molecular dynamics study on the use of deep eutectic solvents for enhanced oil recovery, *J. Pet. Eng.*, 2022, **209**, 109953.
16 A. Kumar, S. Medha, D. Chakraborty, D. Kundu and S. Khan, Enhanced oil recovery promoted by aqueous deep eutectic solvents on silica and calcite surfaces: A molecular dynamics study, *Phys. Chem. Chem. Phys.*, 2025, **27**, 9573–9589.
17 G. L. P. Rao, A. Mandal and N. Pal, Choline chloride-urea based deep eutectic solvent: characterization, interfacial behavior and synergism in binary (surfactant) systems, *Chem. Phys.*, 2025, **588**, 112496.
18 A. Mohsenzadeh, Y. Al-Wahaibi, A. Jibril, R. Al-Hajri and S. Shuwa, The novel use of deep eutectic solvents for enhancing heavy oil recovery, *J. Pet. Eng.*, 2015, **130**, 6–15.
19 O. Shayestehpour and S. Zahn, Molecular features of reline and homologous deep eutectic solvents contributing to

non-ideal mixing behavior, *J. Phys. Chem. B*, 2020, **124**, 7586–7597.
20 M. T. Garcia, N. Gathergood and P. J. Scammells, Biodegradable ionic liquids Part II. Effect of the anion and toxicology, *Green Chem.*, 2005, **7**, 9–14.
21 T. Jahns, H. Ewen and H. Kaltwasser, Biodegradability of urea-aldehyde condensation products, *J. Polym. Environ.*, 2003, **11**, 155–159.
22 C. E. Stauffer, The measurement of surface tension by the pendant drop technique, *J. Phys. Chem.*, 1965, **69**, 1933–1938.
23 J. Drelich, C. Fang and C. White, Measurement of interfacial tension in fluid-fluid systems, *J. Colloid Sci.*, 2002, **3**, 3158–3163.
24 H. Amani, Evaluation of biosurfactants and surfactants for crude oil contaminated sand washing, *J. Pet. Sci. Technol.*, 2015, **33**, 510–519.
25 M. Kharazi, J. Saien, M. Yarie and M. A. Zolfigol, Different spacer homologs of Gemini imidazolium ionic liquid surfactants at the interface of crude oil-water, *J. Mol. Liq.*, 2019, **296**, 111748.
26 J. Saien, A. Eghtenaie and M. Kharazi, Synergistic performance of a Gemini nano ionic liquid and sodium dodecyl sulfate surfactants at the crude oil–water interface, *Arab. J. Chem.*, 2023, **16**, 105329.
27 A. P. Abbott, D. Boothby, G. Capper, D. L. Davies and R. K. Rasheed, Deep eutectic solvents formed between choline chloride and carboxylic acids: versatile alternatives to ionic liquids, *J. Am. Chem. Soc.*, 2004, **126**, 9142–9147.
28 G. R. Jenkin, A. Z. Al-Bassam, R. C. Harris, A. P. Abbott, D. J. Smith, D. A. Holwell, R. J. Chapman and C. J. Stanley, The application of deep eutectic solvent ionic liquids for environmentally-friendly dissolution and recovery of precious metals, *Miner. Eng.*, 2016, **87**, 18–24.
29 K. Sultana, M. T. Rahman, K. Habib and L. Das, Recent advances in deep eutectic solvents as shale swelling inhibitors: a comprehensive review, *ACS Omega*, 2022, **7**, 28723–28755.
30 S. Zhu, H. Li, W. Zhu, W. Jiang, C. Wang, P. Wu, Q. Zhang and H. Li, Vibrational analysis and formation mechanism of typical deep eutectic solvents: an experimental and theoretical study, *J. Mol. Graph.*, 2016, **68**, 158–175.
31 F. Weinhold, C. Landis and E. Glendening, What is NBO analysis and how is it useful?, *Int. Rev. Phys. Chem.*, 2016, **35**, 399–440.
32 E. D. Glendening, C. R. Landis and F. Weinhold, Natural bond orbital methods, Wiley Interdiscip, *Rev. Comput.*, 2012, **2**, 1–42.
33 K. B. Wiberg, Application of the pople-santry-segal CNDO method to the cyclopropylcarbinyl and cyclobutyl cation and to bicyclobutane, *Tetrahedron*, 1968, **24**, 1083–1096.
34 M. Bayat, S. Salehzadeh and G. Frenking, Energy decomposition analysis of the metal-imine bond in $[(CO)_4M–SB]$(M=Cr, Mo, W; SB: $RHCN–CH_2CH_2–NCHR$), *J. Organomet. Chem.*, 2012, **697**, 74–79.
35 S. Salehzadeh, F. Yaghoobi and M. Bayat, Theoretical studies on the interaction of some endohedral fullerenes $\{[X@C_{60}]^-$ ($X = F^-, Cl^-, Br^-$) or $[M@C_{60}]$ ($M = Li, Na, K$)} with $[Al(H_2O)_6]^{3+}$ and $[Mg(H_2O)_6]^{2+}$ cations, *Comput. Theor. Chem.*, 2014, **1034**, 73–79.
36 S. Salehzadeh, M. Bayat and Y. A. Gholiee, Theoretical study on the importance of steric effects, electronic properties, interaction and solvation energies in the 'host–guest' chemistry of protonated azacryptands and halide anions, *Tetrahedron*, 2013, **69**, 9183–9191.
37 A. E. Reed, L. A. Curtiss and F. Weinhold, Intermolecular interactions from a natural bond orbital, donor-acceptor viewpoint, *Chem. Rev.*, 1988, **88**, 899–926.
38 B. Naderizadeh, M. Bayat, M. Ranjbaran and S. Salehzadeh, Towards computational prediction of anti-cancer activity: Making connection between IC_{50} values and metal–ligand interaction energies in some NHC complexes of groups 10 and 11, *J. Mol. Liq.*, 2021, **341**, 117310.
39 M. Mitoraj and A. Michalak, Natural orbitals for chemical valence as descriptors of chemical bonding in transition metal complexes, *J. Mol. Model.*, 2007, **13**, 347–355.
40 P. S. V. Kumar, V. Raghavendra and V. Subramanian, Bader's theory of atoms in molecules (AIM) and its applications to chemical bonding, *Chem. Sci. J.*, 2016, **128**, 1527–1536.
41 R. K. Banjare, M. K. Banjare, K. Behera, S. Pandey and K. K. Ghosh, Micellization behavior of conventional cationic surfactants within glycerol-based deep eutectic solvent, *ACS omega*, 2020, **5**(31), 19350–19362.
42 M. Kharazi, J. Saien, M. Yarie and M. A. Zolfigol, The superior effects of a long chain gemini ionic liquid on the interfacial tension, emulsification and oil displacement of crude oil–water, *J. Pet. Sci. Eng.*, 2020, **195**, 107543.
43 O. S. Hammond and A. V. Mudring, Ionic liquids and deep eutectics as a transformative platform for the synthesis of nanomaterials, *Chem. Commun.*, 2022, **58**, 3865–3892.
44 M. Kharazi, J. Saien and R. Miller, The surface activity of surfactants at liquid interfaces: The role of CMC, decrease in surface tension, HLB, thermodynamic adsorption models, *J. Surfactants Deterg.*, 2025, 1–26.
45 J. Saien, B. Shokri and M. Kharazi, Synergism in mixtures of nano benzimidazolium Gemini ionic liquid and sodium dodecyl sulfate surfactants in tuning interfacial properties of crude oil−water system, *J. Mol. Liq.*, 2023, **391**, 123280.
46 J. Saien, B. Shokri and M. Kharazi, Effective synergistic action of benzimidazolium nano Gemini ionic liquid and conventional surfactant for chemical enhanced oil recovery, *ACS Omega*, 2024, (9), 22336–22344.
47 K. Birdi, *Surface and Colloid Chemistry: Principles and Applications*, CRC Press, 2009.
48 C. Stubenrauch, V. Fainerman, E. Aksenenko and R. Miller, Adsorption behavior and dilatational rheology of the cationic alkyl trimethylammonium bromides at the water/air interface, *J. Phys. Chem. B*, 2005, **109**, 1505–1509.
49 D. Möbius, R. Miller and V. B. Fainerman, *Surfactants: Chemistry, Interfacial Properties, Applications*, Elsevier, 2001.
50 G. Liu, D. Gu, H. Liu, W. Ding, H. Luan and Y. Lou, Thermodynamic properties of micellization of sulfobetaine-type zwitterionic Gemini surfactants in

aqueous solutions: A free energy perturbation study, *J. Colloid Interface Sci.*, 2012, **375**, 148–153.

51 K. Motomura, S. I. Iwanaga, M. Yamanaka, M. Aratono and R. Matuura, Thermodynamic studies on adsorption at interfaces: V. adsorption from micellar solution, *J. Colloid Interface Sci.*, 1982, **86**, 151–157.

52 S. Asadabadi, M. Kharazi and J. Saien, Salinity and alkalinity impacts on the interfacial activity of crude oil–water systems using individual and mixtures of a surface-active ionic liquid and conventional surfactant, *RSC Adv.*, 2025, **15**, 36050–36064.

53 H. Matsubara, A. Onohara, Y. Imai, K. Shimamoto, T. Takiue and M. Aratono, Effect of temperature and counterion on adsorption of imidazolium ionic liquids at air–water interface, *Colloids Surf., A*, 2010, **370**, 113–119.

54 J. Saien and M. Kharazi, *The Properties and Applications of Surface-Active Ionic Liquids: in Properties and Applications of Ionic Liquids*, Nova Science, 2023.

55 L. He, F. Lin, X. Li, H. Sui and Z. Xu, Interfacial sciences in unconventional petroleum production: from fundamentals to applications, *Chem. Soc. Rev.*, 2015, **44**, 5446–5494.

56 Y. Wu, H. Song, Y. Zheng, F. You, S. Chang and S. Zhu, Amphiphilic nitrogen-doped carbon dots derived from bituminous coal: enhanced oil-water interfacial activity and nanomaterial dispersibility, *Fuel Process. Technol.*, 2025, **275**, 108261.

57 X. Wang, Q. Zhang, X. Li, J. Ye and L. Li, Structural and electronic properties of different terminations for quartz (001) surfaces as well as water molecule adsorption on it: a first-principles study, *Minerals*, 2018, **8**, 58.

58 J. H. Guo, Y. F. Bai, L. Du, L. Y. Wei, Y. Zhao, X. B. Zheng, E. L. Yang, Z. G. Wang, H. Huang and W. T. Zhang, Experimental investigation on the effects of deep eutectic solvents (DES) on the wettability of sandstone samples, *J. Pet. Sci.*, 2025, **22**, 1380–1390.